SLC15A4 mediates M1-prone metabolic shifts in macrophages and guards immune cells from metabolic stress

Toshihiko Kobayashi[a,1] , Dat Nguyen-Tien[a,1] , Yuriko Sorimachi[b,c,1], Yuki Sugiura[d,1] , Takehiro Suzuki[e], Hitomi Karyu[a], Shiho Shimabukuro-Demoto[a], Tatsuki Uemura[d], Tadashi Okamura[f], Tomohiko Taguchi[g] , Kohjiro Ueki[h] , Norihiro Kato[i], Nobuhito Goda[c] , Naoshi Dohmae[e], Keiyo Takubo[b] , Makoto Suematsu[d] , and Noriko Toyama-Sorimachi[a,2]

[a]Department of Molecular Immunology and Inflammation, Research Institute, National Center for Global Health and Medicine, Tokyo 162-8655, Japan; [b]Department of Stem Cell Biology, Research Institute, National Center for Global Health and Medicine, Tokyo 162-8655, Japan; [c]Department of Life Science and Medical Bioscience, School of Advanced Science and Engineering, Waseda University, Tokyo 162-8480, Japan; [d]Department of Biochemistry, Keio University School of Medicine, Tokyo 160-8582, Japan; [e]Biomolecular Characterization Unit, RIKEN Center for Sustainable Resource Science, Saitama 351-0198, Japan; [f]Department of Laboratory Animal Medicine, Research Institute, National Center for Global Health and Medicine, Tokyo 162-8655, Japan; [g]Department of Integrative Life Sciences, Graduate School of Life Sciences, Tohoku University, Miyagi 980-8578, Japan; [h]Department of Molecular Diabetic Medicine, Diabetes Research Center, Research Institute, National Center for Global Health and Medicine, Tokyo 162-8655, Japan; and [i]Department of Gene Diagnostics and Therapeutics, Research Institute, National Center for Global Health and Medicine, Tokyo 162-8655, Japan

The amino acid and oligopeptide transporter Solute carrier family 15 member A4 (SLC15A4), which resides in lysosomes and is preferentially expressed in immune cells, plays critical roles in the pathogenesis of lupus and colitis in murine models. Toll-like receptor (TLR) 7/9- and nucleotide-binding oligomerization domain-containing protein 1 (NOD1)-mediated inflammatory responses require SLC15A4 function for regulating the mechanistic target of rapamycin complex 1 (mTORC1) or transporting L-Ala-γ-D-Glu-meso-diaminopimelic acid, IL-12: interleukin-12 (Tri-DAP), respectively. Here, we further investigated the mechanism of how SLC15A4 directs inflammatory responses. Proximity-dependent biotin identification revealed glycolysis as highly enriched gene ontology terms. Fluxome analyses in macrophages indicated that SLC15A4 loss causes insufficient biotransformation of pyruvate to the tricarboxylic acid cycle, while increasing glutaminolysis to the cycle. Furthermore, SLC15A4 was required for M1-prone metabolic change and inflammatory IL-12 cytokine productions after TLR9 stimulation. SLC15A4 could be in close proximity to AMP-activated protein kinase (AMPK) and mTOR, and SLC15A4 deficiency impaired TLR-mediated AMPK activation. Interestingly, SLC15A4-intact but not SLC15A4-deficient macrophages became resistant to fluctuations in environmental nutrient levels by limiting the use of the glutamine source; thus, SLC15A4 was critical for macrophage's respiratory homeostasis. Our findings reveal a mechanism of metabolic regulation in which an amino acid transporter acts as a gatekeeper that protects immune cells' ability to acquire an M1-prone metabolic phenotype in inflammatory tissues by mitigating metabolic stress.

innate immune cell | immunometabolism | amino acid transporter | cytokine | macrophage

Innate immune cells, including monocytes and dendritic cells, infiltrate inflamed tissues and mediate immune responses despite drastic changes in nutrient availability, low partial oxygen pressure, and other environmental stresses. Immune cells adapt to these environmental stresses by changing their metabolic state, and this adaptation is vitally important for these cells to fulfill their function in the immune system (1, 2). Solute carrier family 15 member 4 (SLC15A4) is a proton-coupled amino acid/oligopeptide transporter that is preferentially expressed in hematopoietic lineage cells such as macrophages, B cells, and plasmacytoid dendritic cells (3–5). This transporter, which localizes mainly in LAMP1+ vesicular compartments such as late endosomes and lysosomes, is required for Toll-like receptor (TLR)7- and TLR9-dependent production of cytokines such as type I interferon (IFN-I) and interleukin (IL)-6

(4, 6–8) and plays a critical role in autoimmune and other inflammatory diseases (3, 6, 9). SLC15A4 colocalizes with the mechanistic target of rapamycin (mTOR) (3, 10), and SLC15A4's effects on TLR7 and TLR9 signaling are partly mediated through the regulation of mTORC1 activity (3).

To understand SLC15A4's mode of action in detail, we used BioID to identify molecules that are in close proximity to SLC15A4 (11, 12) using 293T transfectants expressing SLC15A4 proteins fused with BirA biotin ligase at the N terminus and used membrane raft-targeting methionine-glycine-cysteine (MGC) peptides (13) fused with BirA as a control (SI Appendix, Fig. S1 A–D). A large number of biotinylated proteins were precipitated from cells expressing BirA-SLC15A4 but not from parental 293T or cells

Significance

SLC15A4 is a lysosome-resident amino acid/oligopeptide transporter that is preferentially expressed in immune cells. SLC15A4 is required for TLR7/9-dependent type I interferon production and plays a critical role in the pathogenesis of lupus and colitis. However, the precise molecular mechanisms of SLC15A4-mediated inflammatory responses are still undetermined. We revealed that SLC15A4 loss disturbed the coupling of glycolysis and the TCA cycle, and SLC15A4-deficient macrophages preferred to use glutamine rather than glucose as a carbon source for the TCA cycle. SLC15A4-deficient macrophages produced low levels of itaconate and proinflammatory IL-12 cytokine members. Our results reveal a mechanism of metabolic regulation in which an amino acid transporter acts as a guardian to allow macrophages to acquire an M1-prone metabolic phenotype.

expressing control-BirA (Fig. 1*A*). Mass spectrometry identified 424 precipitated proteins that increased more than twofold in cells expressing BirA-SLC15A4 compared with those expressing control-BirA (project accession: PXD020370) (14). Among SLC15A4-dependent biotinylated proteins, we identified nine proteins involved in the mTOR signaling pathway, including RagA, RagB, RagC, and Lamtor1/2 (Fig. 1*B* and *SI Appendix*, Fig. S1 *E* and *F*). SLC15A4 itself was among the molecules with the highest scores, indicating that we had

successfully collected proteins biotinylated by BirA-SLC15A4 (Fig. 1*B*). Functional annotation analyses of mass spectrometry datasets identified 15 biological processes associated with the enriched proteins, including glucose metabolism/glycolysis in SLC15A4's profile (Fig. 1*C*). We then examined SLC15A4's role in glycolysis using human plasmacytoid dendritic cell line CAL-1 (15). SLC15A4 knockdown CAL-1 cells (CAL-1-shA4) showed the significant reduction of SLC15A4 expression (*SI Appendix*, Fig. S2 *A* and *B*), and TLR9-mediated *IFNB1* expressions
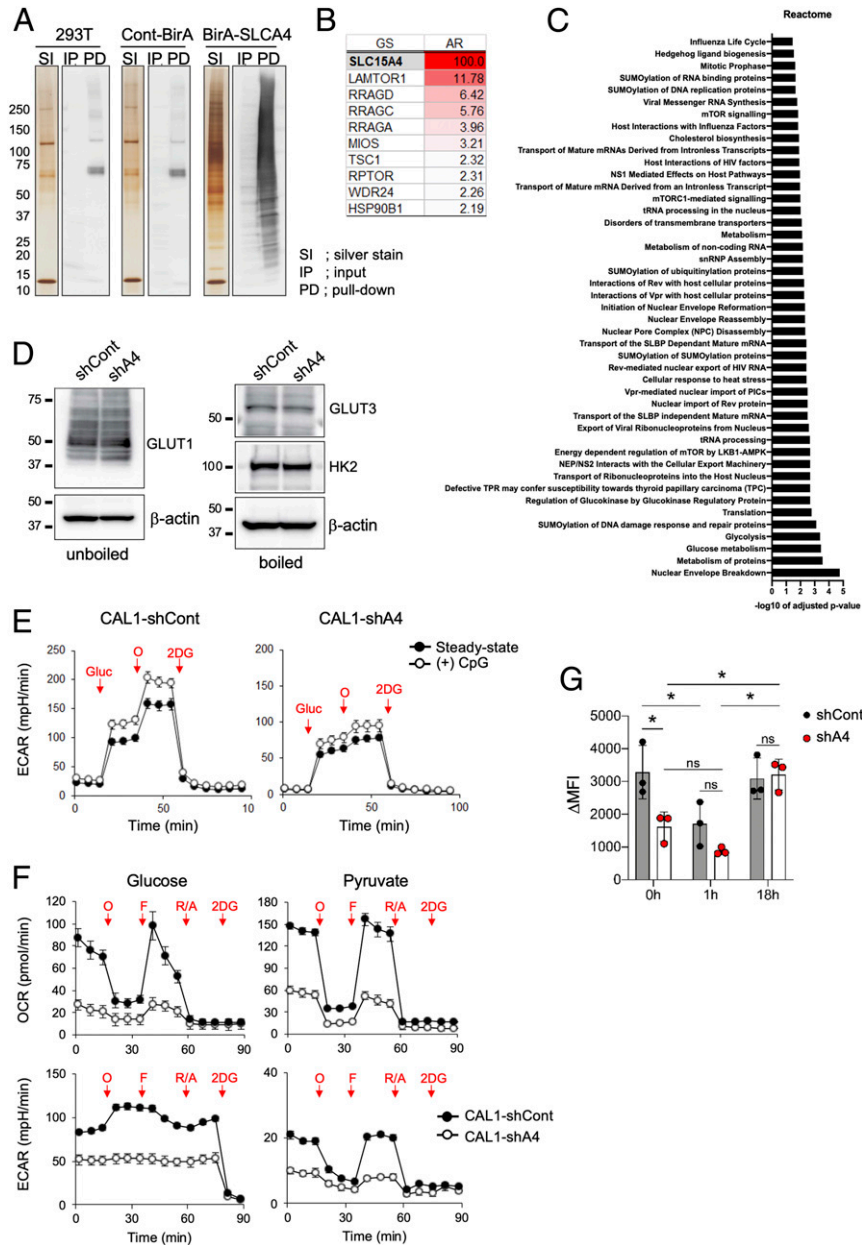

Fig. 1. Identification of SLC15A4-associated molecules by BioID. (*A*) Precipitation of SLC15A4-interacting proteins. Biotinylated precipitates were visualized by silver staining or by Western blot. (*B*) The enrichment of SLC15A4-interacting proteins involved in the mTOR pathway. Abundance ratio (AR) score: relative enrichment value over the control. (*C*) Pathway analysis of SLC15A4-interacting proteins by g:Profiler (https://biit.cs.ut.ee/gprofiler/gost). (*D*) Expression of glycolysis-related proteins in CAL-1-shCont or CAL-1-shA4 cells was analyzed by Western blotting. (*E* and *F*) Seahorse XF analysis of OCR and ECAR. (*E*) OCR and ECAR in CAL-1 cells were compared between the presence or absence of CpG stimulation in Seahorse XF basic RPMI medium containing 2 mM glutamine. Reagents were added at the indicated time points (arrows). (*F*) OCR (*Upper*) and ECAR (*Bottom*) were compared between CAL-1-shCont and CAL-1-shA cells in the presence of 10 mM glucose (*Left*) or 2 mM pyruvate (*Right*) by Mito Stress Test using Seahorse XF basic RPMI medium. (*G*) Glucose uptake assay was performed for CAL-1-shCont or CAL-1-shA4 cells treated with CpG-B (ODN2006) for the indicated periods. Uptake of 2-NBDG (a fluorescent D-glucose analog) was evaluated by fluorescence intensity within cells using flow cytometry. The results are representative of three independent experiments. *$P < 0.05$, as determined by one-way ANOVA followed by Tukey's post hoc test.

was almost completely absent in CAL-1-shA4 (*SI Appendix*, Fig. S2C), consistent with previous observations (3, 6, 8, 16). Although we detected the decreased gene expression of glucose transporter 1 (*GLUT1*) in CAL-1-shA4 compared with CAL-1-shCont cells (*SI Appendix*, Fig. S2D), the protein expression levels of GLUT 1, GLUT 3, and HK2 were not affected by the presence or absence of SLC15A4 (Fig. 1D). We further assessed cellular glycolytic activities by measuring the extracellular acidification rate (ECAR) and oxygen consumption rate (OCR) with a Seahorse XF Extracellular Flux Analyzer (17). In Glyco Stress Tests, the addition of glucose increased ECAR in both CAL-1-shCont and CAL-1-shA4 cells (Fig. 1E). The addition of oligomycin further increased ECAR in CAL-1-shCont cells irrespective of the presence or absence of TLR stimulation (Fig. 1E), suggesting that pyruvate, the end product of glycolysis, enters the mitochondria for oxidative phosphorylation (OXPHOS), and oligomycin treatment causes an elevated pyruvate flux toward lactate. In contrast, oligomycin had little effect on ECAR in CAL-1-shA4 cells (Fig. 1E). These results indicated that CAL-1-shA4 had a lower glycolytic reserve than CAL-1-shCont. Basal OCR and ECAR were lower in CAL-1-shA4 cells than in CAL-1-shCont cells in both the presence and absence of pyruvate (Fig. 1F). Similar trends were observed when only glucose was used as a carbon source (Fig. 1F). Oligomycin and (trifluoromethoxy) phenylhydrazone (FCCP) decreased and increased OCR, respectively, in CAL-1-shCont, with a concomitant change in ECAR (Fig. 1F). However, neither oligomycin nor FCCP affected ECAR in CAL-1-shA4 cells when glucose was used as a carbon source (Fig. 1F). These results suggested dysregulation of the coupling between OXPHOS and glycolysis in CAL-1-shA4 cells. When pyruvate was used as a carbon source, OCR and ECAR were concomitantly changed by oligomycin or FCCP, although ECAR values were lower in both CAL-1-shA4 and CAL-1-shCont cells compared with when glucose was used (Fig. 1F). Glucose uptake in CAL-1-shA4 cells was lower compared with CAL-1-shCont cells in a steady state but was comparable to CAL-1-shCont cells after CpG stimulation (Fig. 1G). Thus, although the decreased glycolytic activity in CAL-1-shA4 cells was partly explained by the decreased uptake of glucose, it was also possible that SLC15A4 contributed to the coordinated regulation between glycolysis and OXPHOS.

The dysregulation of glucose use in CAL-1-shA4 cells compared with CAL-1-shCont cells was consistent with our recent report, whereby we found that CAL-1-shA4 promptly decreased mitochondria membrane potential in amino acid–starved conditions in which glucose was included as the carbon source in Earle's Balanced Salt Solution medium (16). Therefore, we further examined the role of SLC15A4 by focusing on the coupling between glycolysis and the tricarboxylic acid (TCA) cycle in additional cell types. Macrophages change the metabolic state in response to environmental cues such as infectious stimuli and the availability of nutrients, and this dynamic metabolic reprograming is vitally important in macrophages' functional polarization (2, 18). In Glyco Stress Tests using bone marrow–derived macrophages (BMMϕ), *Slc15a4−/−* BMMϕ showed larger ECAR and OCR than *Slc15a4+/+* BMMϕ in the steady state (Fig. 2A). TLR9 or TLR4 stimulation increased ECAR in both *Slc15a4+/+* and *Slc15a4−/−* BMMϕ (Fig. 2A), consistent with previous observations that macrophages shift to glycolysis after stimulation (2, 18). These results indicated that SLC15A4 is not required for a metabolic switch toward glycolysis after stimulation. It should be noted that *Slc15a4+/+* BMMϕ showed increased OCR with a concomitant increase in ECAR after TLR9 or TLR4 stimulation (Fig. 2A). In contrast, OCR in *Slc15a4−/−* BMMϕ were nearly unchanged after stimulation even though ECAR increased (Fig. 2A). The protein expression of enzymes involved in pyruvate metabolism, such as lactate dehydrogenase A (LDHA), pyruvate dehydrogenase (PDH), and succinate dehydrogenase complex flavoprotein subunit A (SDHA), were not largely affected by SLC15A4 loss, although a slight decrease in LDHA was detectable

at 18 h after stimulation in *Slc15a4−/−* BMMϕ (*SI Appendix*, Fig. S3A). These results suggested that *Slc15a4+/+* BMMϕ increased the mitochondrial pyruvate flux of OXPHOS after inflammatory stimulation, while in *Slc15a4−/−* BMMϕ, mitochondrial pyruvate flux was not changed before and after stimulation even though it increased glycolysis.

We further examined SLC15A4's effect on glucose metabolism more directly by metabolic flux analysis using $^{13}C_6$-glucose and $^{13}C_5$-glutamine. Principal component analyses of metabolites showed wide differences in metabolite intermediates produced by *Slc15a4+/+* and *Slc15a4−/−* BMMϕ, particularly after CpG stimulation (Fig. 2B). Most glycolysis intermediates were elevated 1 h after CpG treatment in both *Slc15a4+/+* and *Slc15a4−/−* BMMϕ (Fig. 2C). Pyruvate and lactate levels were higher in *Slc15a4−/−* BMMϕ than in *Slc15a4+/+* BMMϕ 18 h after treatment (Fig. 2 C and E). Glucose uptake was not strikingly different between *Slc15a4+/+* and *Slc15a4−/−* BMMϕ, although the latter showed a slight decrease in its uptake (*SI Appendix*, Fig. S3B). Notably, acetyl-CoA levels 18 h after stimulation were significantly decreased in *Slc15a4−/−* BMMϕ compared with *Slc15a4+/+* BMMϕ (Fig. 2F). The observation that glucose-derived citrate decreased and pyruvate accumulated in the absence of SLC15A4 was consistent with this observation (Fig. 2 C and E). Succinate was increased 18 h after CpG stimulation in both *Slc15a4+/+* and *Slc15a4−/−* BMMϕ, although glucose-derived succinate was decreased in *Slc15a4−/−* BMMϕ compared with *Slc15a4+/+* BMMϕ (Fig. 2 C and E). However, succinate from glutamine was more increased in *Slc15a4−/−* BMMϕ than in *Slc15a4+/+* BMMϕ (Fig. 2 D and E), suggesting that SLC15A4 loss prevented the smooth integration of glycolysis with the TCA cycle, causing *Slc15a4−/−* BMMϕ to draw more glutamine into the TCA cycle. Importantly, phosphorylation of the PDH E1 component subunit alpha PDHA at S293 was increased in *Slc15a4−/−* BMMϕ (Fig. 2G). Since PDHA activity is suppressed by the phosphorylation of S293 by PDHK, this observation was consistent with the decreased acetyl-CoA in *Slc15a4−/−* BMMϕ. The same trend of PDHA S293 phosphorylation was observed in alveolar Mϕs (*SI Appendix*, Fig. S3C), strongly suggesting that SLC15A4 mediates the conversion of pyruvate to acetyl-CoA not only in BMMϕ but also in a certain type of tissue-resident macrophage. Taken together, these results indicated that SLC15A4 increased the efficiency of acetyl-CoA formation by controlling PDH activity. More interestingly, *Slc15a4−/−* BMMϕ produced significantly low levels of itaconate and transaconitate (Fig. 2H), metabolites that are produced in response to the stimulation-dependent interruption of the TCA cycle in M1 macrophages (19–21). Particularly, itaconate not only has antibacterial activity but also regulates a panel of gene expression associated with immune regulation (21). Thus, these observations revealed that SLC15A4 loss impaired M1-prone metabolic changes and probably the acquisition of M1-associated effector functions after stimulation.

We next investigated the significance of SLC15A4-mediated metabolic regulation in Mϕ inflammatory responses and found that CpG-stimulated *Slc15a4−/−* BMMϕ showed the severe decrease of *Il12b* and *Il27* expression (Fig. 3A). IL-12 cytokine family uses two different β chains, IL-12/23 p40 (*Il12b*) and Ebi3, and covers a very broad range of immune responses including proinflammatory to anti-inflammatory responses (22). The expression of *Ebi3* was less influenced, and *Il12a* and *Il23a* expressions were rather increased in *Slc15a4−/−* BMMϕ (Fig. 3A). *Tnf* was not affected by the presence or absence of SLC15A4, although *Il6* was increased (Fig. 3B). These results in BMMϕ were inconsistent with previous studies of B cells and dendritic cells (3, 4). Because BMMϕ were stimulated with CpG in the presence of macrophage colony-stimulating factor (M-CSF), by which PI3K–AKT-mediated signaling events are continuously transmitted, it was likely that the effect of SLC15A4 loss on inflammatory responses differed between cell types depending on
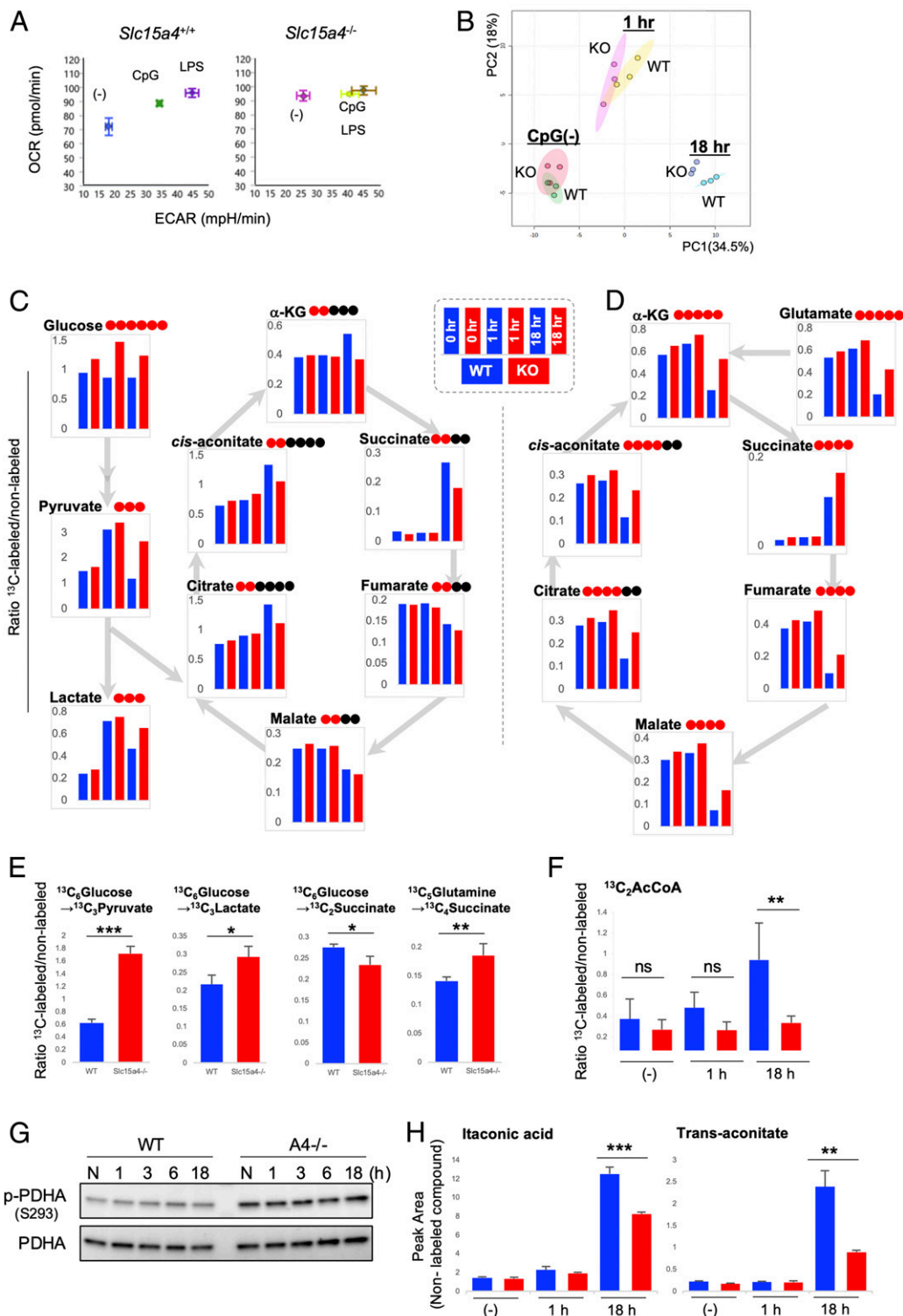
Kobayashi et al.
SLC15A4 mediates M1-prone metabolic shifts in macrophages and guards immune cells from metabolic stress

PNAS | 3 of 10
https://doi.org/10.1073/pnas.2100295118

IMMUNOLOGY AND INFLAMMATION

www.manaraa.com

Fig. 2. Metabolic analyses in BMMφ. (*A*) Energy map of Seahorse XF Glyco stress test. BMMφ were stimulated with the indicated TLR agonists for 2 h in complete RPMI containing 10% fetal calf serum. Data showed OCR and ECAR 15 min after the addition of glucose. (*B*) Principal component analysis of metabolites in the steady state (0 h) 1 and 18 h after CpG stimulation (*n* = 3). (*C* and *D*) Summary of metabolic flow analyses using $^{13}C_6$-glucose and $^{13}C_5$-glutamine. BMMφ stimulated with CpG for 1 or 18 h were incubated for 1 h in the presence of $^{13}C_6$-glucose (*C*) and $^{13}C_5$-glutamine (*D*), and metabolic intermediates in glycolysis and the TCA cycle were quantified by MS. Values in bar graphs represent the ratio between ^{12}C and ^{13}C, and the reference of graphs was shown in *Bottom Left*. Red and closed circles in individual metabolites denote the numbers of ^{13}C and ^{12}C in the metabolites. References of graphs were shown in the area surrounded by dotted lines. (*E*) Bar graphs of statistical differences in the indicated metabolites (*n* = 3). *$P < 0.05$, **$P < 0.01$, ***$P < 0.001$ as determined by Student's two-tailed *t* test. (*F*) Measurement of acetyl-CoA. The ratio of $^{13}C_6$-glucose–derived acetyl-CoA was calculated and shown as bar graphs of statistical differences (*n* = 3). **$P < 0.01$. (*G*) Phosphorylation of PDHA at Ser293 was compared between wild-type (WT) and *Slc15a4*$^{-/-}$ BMMφ. WT or *Slc15a4*$^{-/-}$ BMMφ were cultured and stimulated with CpG1668 for the indicated periods. (*H*) The ratio of Itaconic acid and transaconitate derived from $^{13}C_6$-glucose and $^{13}C_5$-glutamine (*n* = 3). Data are representative of two independent experiments.

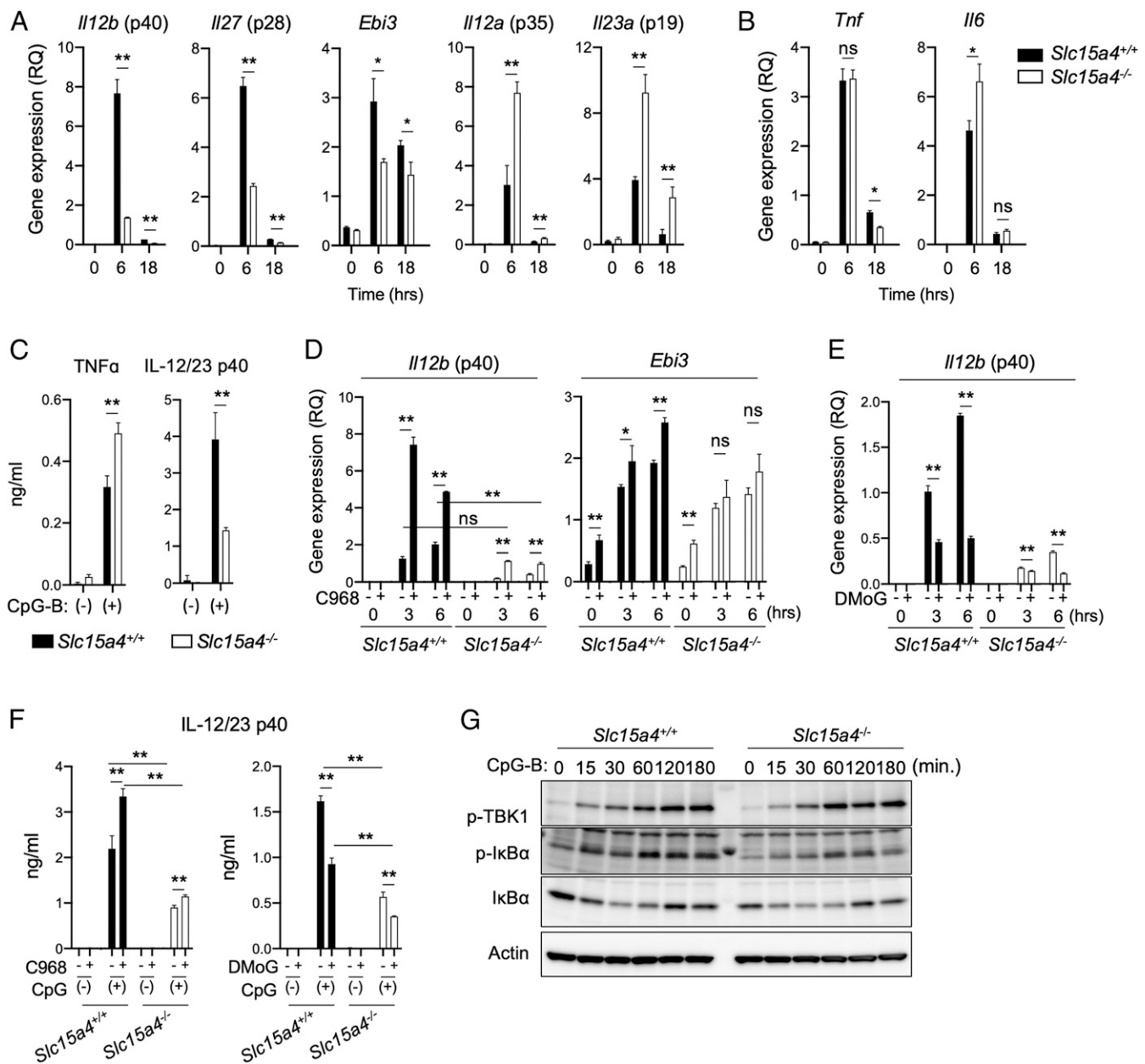https://doi.org/10.1073/pnas.2100295118

Fig. 3. Effect of glutaminolysis on the production of IL-12 family cytokines in Mϕ. BMMϕ stimulated with CpG1668 in 10% fetal calf serum–containing medium were analyzed. (*A*) Gene expressions of IL-12 family members after CpG1668 stimulation in BMMϕ were analyzed by RT-PCR. (*B*) Gene expressions of *Tnf* or *Il6* after CpG1668 stimulation in BMMϕ were analyzed by RT-PCR. (*C*) TNF-α and IL-12/23p40 productions by BMMϕ. Wild-type (WT) or *Slc15a4*⁻/⁻ BMMϕ were cultured and stimulated with CpG1668 for 18 h, and the culture supernatant was subjected to ELISA. (*D* and *E*) Gene expressions of *Il12b* or *Ebi3* after CpG1668 stimulation for the indicated periods in the presence of Glutaminase inhibitor 968 (appeared as C968 in *D*) or Dimethyl-α-oxo-glutarate (appeared as DMoG in *E*) in BMMϕ were analyzed by RT-qPCR. (*F*) Effect of glutaminolysis modulation on IL-12/23p40 production by BMMϕ. WT or *Slc15a4*⁻/⁻ BMMϕ were stimulated with CpG1668 for 18 h in the presence or absence of C968 glutaminase inhibitor or DMoG, and the culture supernatant was analyzed by ELISA. (*G*) Western blot analysis of the CpG-triggered signaling in BMMϕ. *$P < 0.05$, **$P < 0.01$, ns, not significant, as determined by Student's two-tailed *t* test. Data are representative of at least two independent experiments.

the crosstalk with other signaling pathways. The decreased production of IL-12/23 p40 was also confirmed at the protein level (Fig. 3*C*). These results indicated the selective requirement of SLC15A4 in the expression of IL-12 family members. We further investigated the interrelation between the suppression of *Il12b* and the metabolic change caused by SLC15A4 loss. Since *Slc15a4*⁻/⁻ BMMϕ showed the increased use of glutamine for TCA cycle, we used Compound 968 (C968), an inhibitor of glutaminase, to inhibit the conversion from glutamine to glutamate, which can be further metabolized to α-ketoglutarate, resulting in blocking the

replenishment of glutamine-derived α-ketoglutarate. In the presence of C968, *Il12b* expression augmented in both *Slc15a4*⁺/⁺ and *Slc15a4*⁻/⁻ BMMϕ (Fig. 3*D*). Although *Il12b* expression induced by C968 in *Slc15a4*⁻/⁻ BMMϕ was lower than that in *Slc15a4*⁺/⁺ BMMϕ, C968 increased *Il12b* expression in *Slc15a4*⁻/⁻ BMMϕ to similar levels of *Il12b* in C968-untreated *Slc15a4*⁺/⁺ BMMϕ, suggesting the contribution of glutaminolysis to the decreased *Il12b* in *Slc15a4*⁻/⁻ BMMϕ. At the same time, these results implied a multifaceted contribution of glutaminolysis to *Il12b* expression because *Il12b* expression in *Slc15a4*⁺/⁺ BMMϕ was also

inhibited by C968. In contrast, *Ebi3* expression was almost not changed by the C968 treatment (Fig. 3*D*). Conversely, the addition of dimethyl-oxoglutarate (dimethyl-α-ketoglutarate, DMoG) suppressed *Il12b* expression (Fig. 3*E*). The effects of C968 and DMoG on IL-12/23 p40 protein expression showed similar trends to *Il12b* gene expression, although the influence on protein expression became smaller than those on gene expression (Fig. 3*F*). We did not observe a severe defect in TLR9-mediated canonical signaling events in *Slc15a4*$^{-/-}$ BMMφ (Fig. 3*G*), consistent with the normal ranges of the TNF-α production by *Slc15a4*$^{-/-}$ BMMφ (Fig. 3 *B* and *C*). These results strongly suggested that the SLC15A4-dependent restriction of glutamine replenishment is critical for the selectivity of IL12 family cytokine expressions.

During metabolic analyses, we noticed that respiratory functions in *Slc15a4*$^{-/-}$ BMMφ were easily influenced by serum concentration in culture medium. While *Slc15a4*$^{+/+}$ BMMφ maintained the OCR and ECAR rates at a certain level regardless of the concentration of serum in the culture medium, *Slc15a4*$^{-/-}$ BMMφ changed OCR and ECAR more sensitively depending on serum concentration, and *Slc15a4*$^{-/-}$ BMMφ possessed higher respiratory reservation than *Slc15a4*$^{+/+}$ BMMφ in low serum concentration (Fig. 4 *A* and *B*). These observations implied that SLC15A4 is critical for the macrophage's respiratory homeostasis by adapting their metabolic state to different nutrient conditions. Since a macrophage's nutrient environment changes drastically upon inflammation, the ability of *Slc15a4*$^{+/+}$ BMMφ to maintain respiratory homeostasis is likely important to enhance their competence for fulfilling inflammatory responses. In addition, OXPHOS generates reactive oxygen species through mitochondrial activity, which has to occur in the controlled manner to avoid host cell damage. We therefore examined the mechanism of respiratory fragility in *Slc15a4*$^{-/-}$ BMMφ by focusing on glutaminolysis and observed that the fragility in respiratory potential was abrogated in the absence of glutamine (Fig. 4*C*). These results indicated that SLC15A4 is required for macrophage metabolic homeostasis by limiting the availability of glutamine for the TCA cycle.

We finally investigated how SLC15A4 affects glutamine metabolism for the TCA cycle. Previous studies reported that glucose limitation causes the AMPK-dependent augmentation of glutaminolysis in T cells (23). AMPK plays a key role in controlling catabolic responses and mitochondrial respiratory function by sensing ATP levels (24, 25). Recent studies demonstrating that AMPK functions at lysosomes (26, 27) prompted us to examine functional relationships between SLC15A4 and AMPK. We compared AMPK activity between the presence or absence of SLC15A4 and found that AMPK-α phosphorylation in the steady state appeared to be increased in *Slc15a4*$^{-/-}$ BMMφ irrespective of serum concentration (Fig. 4*D*). This might be explained by the decreased mTORC1 activity in *Slc15a4*-deficient cells (3, 10) and possibly contributes to the increase of glutamine replenishment. Unexpectedly, *Slc15a4*$^{-/-}$ BMMφ severely impaired TLR9-induced AMPK-α activation (Fig. 4*D*). The phosphorylation of acetyl-CoA carboxylase (ACC) 1/2, the major AMPK substrate, was not affected by the presence or absence of SLC15A4 (Fig. 4*D*). AMPK-α phosphorylation was entirely absent also in CAL-1-shA4 cells after TLR9 or TLR7 stimulation (*SI Appendix,* Fig. S4). TLR9-dependent AMPK phosphorylation is mediated by TAK1 and involved in actin remodeling through Rho/Rock phosphorylation (28). TLR9-induced inflammatory response is ATP-consuming processes and reduces energy substrate, leading to AMPK activation (29). AMPK activation switches off some ATP-consuming processes and therefore is important to increase the cellular tolerance against the metabolic stress (24). The activities of AMPK and mTORC1 after TLR9 stimulation were differently controlled by the presence or absence of SLC15A4 (Fig. 4*D*), indicating that the balance between anabolic and catabolic metabolism after receiving TLR9 stimulation was not correctly regulated in the absence of SLC15A4. We also found that

AMPK-α was coprecipitated with SLC15A4 (Fig. 4*E*). SLC15A4 precipitates also included mTOR and phosphorylated TAK1, and TLR9 stimulation increased the amount of mTOR in the precipitate (Fig. 4*E*). The association of SLC15A4 and AMPK appeared to be constitutive since it did not differ between the CpG-stimulated and steady states (Fig. 4*E*). The reconstitution experiments using 293T cells showed that both human and murine SLC15A4 interacted with AMPK-α, although murine SLC15A4 interacted more efficiently than human SLC15A4 (Fig. 4*F*). SLC15A4's transporter activity seemed not to be important for AMPKα interaction since the SLC15A4 E465K mutant, which exhibited a severe decrease in transporter activity (3, 16), also could interact with AMPK-α (Fig. 4*F*). Although TAK1 and AMPK were not identified in BioID, it is possible that SLC15A4 interacts with these molecules via interactions with mTORC1 (30, 31). Taken together, our observations revealed a regulation in M1 macrophage function in which SLC15A4 guards immune cells from metabolic stress by controlling both mTORC1 and AMPK.

Our results demonstrated that SLC15A4 plays a vitally important role in the metabolic regulation of innate immune cells such as DCs and macrophages. SLC15A4 enables glycolysis to integrate efficiently with the TCA cycle by governing the acetyl-CoA supply. SLC15A4-deficient macrophages increase glutamine use probably to compensate for carbon in the TCA cycle. Glutamine is an important source of carbon and nitrogen, both of which are also important for massively proliferating cells such as growing tumor cells and clonally expanding T cells (32–34). Furthermore, glutamine metabolism is required for alternative activated macrophages (M2a) and for monocyte epigenetic reprogramming (35, 36), and a lack of glutamine and glutaminolysis augments M1-prone, proinflammatory metabolic changes (35). Therefore, the steady-state expression of SLC15A4 in these innate immune cells safeguards their ability to adapt their metabolic function to the proinflammatory state by connecting glycolysis and the TCA cycle concomitantly with the restriction of glutaminolysis (*SI Appendix,* Fig. S5). Intriguingly, the use of glutamine to fuel the TCA cycle is also critical for inducing trained immunity (innate immune memory) through the fumarate-dependent regulation of histone demethylases (37). Therefore, SLC15A4's effect on glutaminolysis also may play a role in trained immunity. In this context, the observation that glutaminolysis largely affected the expression of IL-12 cytokine members might be important. Given that SLC15A4 is critical for IL-12/23 p40 expression partly by restricting glutaminolysis, it is likely that the *Il12b* gene locus in *Slc15a4*$^{+/+}$ BMMφ is released from glutaminolysis-dependent epigenetic suppression.

Our findings also revealed the critical role of SLC15A4 in developing the tolerance against metabolic stress by controlling AMPK and mTORC1 activities. Both mTORC1 and AMPK probably exist in close proximity to SLC15A4, and SLC15A4 may support the crosstalk and/or cooperative regulation of these molecules by providing a scaffold. Thus, SLC15A4 might be one of key molecules for integrating the immune and metabolic circuit to induce appropriate adaptive responses in macrophages, and expressing SLC15A4 gives macrophages an important advantage when responding to inflammatory stimulation in any milieu.

In summary, SLC15A4 plays novel and important roles in the link between glycolysis and the TCA cycle and in M1-prone metabolic reprogramming. SLC15A4 is critical for the expression of inflammatory IL-12 cytokine members by restricting glutamine replenishment to the TCA cycle. Furthermore, SLC15A4 maintains cellular respiratory homeostasis and increases cells' resistance to metabolic stress. Thus, SLC15A4 may stand guard over metabolic resilience in both human and mouse innate immune cells. Our findings shed light on a mechanism of how macrophages exert their functions in the presence of metabolic stress during inflammation and, at the same time, raise a number of intriguing questions relating to the cooperative regulation of anabolic and
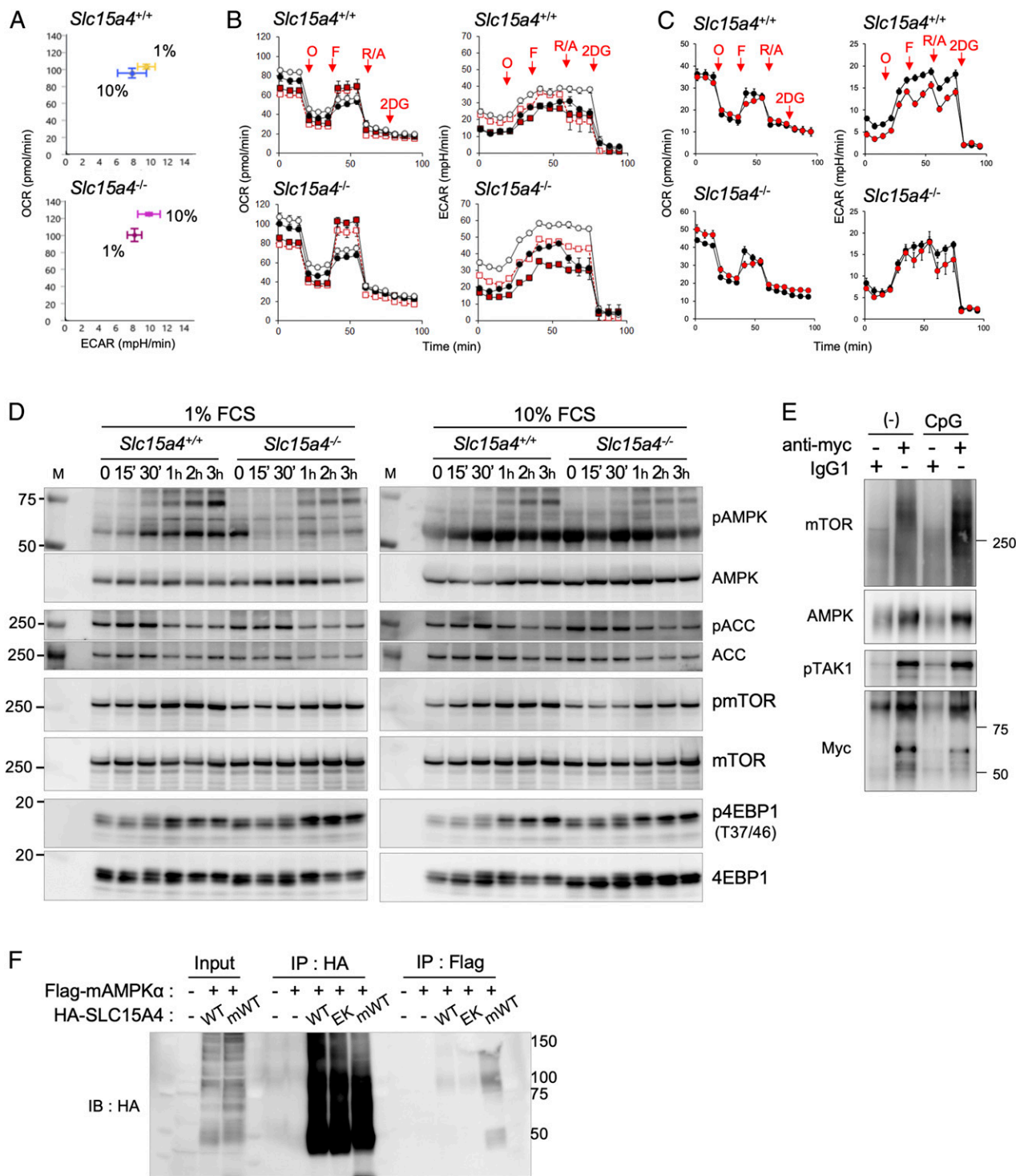
Fig. 4. SLC15A4-mediated resistance to nutrient stress. (*A*) Energy maps of Seahorse XF Mito stress test. OCR and ECAR of BMMφ in different nutrient conditions were measured. The assay medium used was Seahorse XF basic RPMI containing 10% or 1% fetal calf serum (FCS). (*B*) Data showed values of ECAR and OCR 6 h after CpG stimulation measured by Mito Stress Test. BMMφ were treated with CpG1668 (open circles) or control medium (closed circles) for 6 h in the presence of 10% (red squares) or 1% (black symbols) FCS. Before starting assay, media were changed to the assay medium (Seahorse XF basic RPMI medium containing 10% or 1% FCS with 10 mM glucose and 2 mM glutamine). (*C*) Data showed values of ECAR and OCR of BMMφ in the steady state. BMMφ were cultured for 6 h in the presence of 10% (red squares) or 1% (black symbols) FCS without glutamine. Assay medium used was Seahorse XF basic RPMI containing 1% or 10% FCS and 10 mM glucose without glutamine. (*D*) Immunoblotting of BMMφ stimulated with CpG1668 for the indicated periods in different nutrient conditions. (*E* and *F*) Association between SLC15A4 and AMPK. (*E*) Myc-tagged SLC15A4 was precipitated from WEHI231-SLC15A4 transfectants using anti-myc or isotype-matched antibodies, and precipitates were analyzed by Western blot using the indicated antibodies. (*F*) HEK293T cells transiently expressing Flag-tagged mouse AMPK-α in combination with the indicated HA-tagged SLC15A4 proteins (Wild type [WT], EK, or mWT for human WT SLC15A4, human E465K, or mouse WT, respectively) were collected. After lysis, samples were subjected to HA or Flag immunoprecipitation and immunoblotting for the HA-tagged proteins. Data are representative of at least two independent experiments.

Kobayashi et al.
SLC15A4 mediates M1-prone metabolic shifts in macrophages and guards immune cells from metabolic stress

PNAS | 7 of 10
https://doi.org/10.1073/pnas.2100295118

catabolic responses during inflammation. Since tissue-resident Mϕs contain highly diverse populations in vivo, further careful and detailed analyses using various types of tissue-resident Mϕs are required to clarify the significance of SLC15A4-mediated metabolic regulations in unique functional properties of tissue-resident Mϕs. On the basis of our present findings, it will be an interesting future issue to examine *Slc15a4*$^{-/-}$ in inflammatory/infection models in which Mϕs/monocytes play pivotal roles in pathological conditions.

Materials and Methods

Cell Culture. We obtained the CAL-1 human plasmacytoid dendritic cell line (CAL-1 cells) (15) from T. Maeda of Nagasaki University, Nagasaki, Japan. CAL-1 cells were cultured in Roswell Park Memorial Institute (RPMI) 1640 Complete Medium (Sigma-Aldrich) supplemented with 10% (vol/vol) fetal bovine serum (FBS), 10 mM 2-mercaptoethanol, 2 mM L-glutamine, 1 mM sodium pyruvate, 2 mM nonessential amino acids, 1% penicillin G/streptomycin, and 10 mM Hepes (pH 7.0) in a humidified incubator at 37 °C with 5% CO_2. Control and SLC15A4-silenced CAL-1 cells (which appeared in the main text as CAL-1-shCont and CAL-1-shA4 cells, respectively) or SLC15A4-silenced Raji cells (38) were established by transducing the cells with a retrovirus expressing non-targeting short hairpin RNA (shRNA) or expressing SLC15A4 shRNA (pSIREN-RetroQ DsRed, TaKaRa) targeted to the sequence 5′-CUUUGGGAA-CAUCAACAAU-3′, located at the 3′ untranslated region of the *SLC15A4* gene. Human embryonic kidney 293T cells were maintained in Dulbecco's Modified Eagle Medium containing 10% FBS and 1% penicillin G/streptomycin at 37 °C at 5% CO_2. BMMϕ were differentiated from bone marrow (BM) mononuclear cells in the presence of murine M-CSF (50 ng/mL) as described previously (39). Alveolar Mϕs were harvested by bronchoalveolar lavage. Fluids from the bronchoalveolar lavage (BALF) were collected with warmed phosphate-buffered saline (PBS) containing 2 mM ethylenediaminetetraacetic acid and 0.5% FBS and stored on ice. Cells were plated at a density of 4×10^5 cells/well in a 24-well plate with complete RPMI 1640 medium supplemented with 20 ng/mL recombinant mouse granulocyte–macrophage-colony stimulating factor (PeproTech) and stimulated with *Escherichia coli* lipopolysaccharides (Sigma-Aldrich) (1 μg/mL) in combination with IFN-γ (20 ng/mL) (PeproTech) for 24 h. We confirmed by flow cytometry that more than 95% of BALF cells were alveolar Mϕs.

Mice. C57BL/6 *Slc15a4*$^{-/-}$ mice were described previously (6). C57BL/6J mice were purchased from Japan CLEA. All animal experiments were approved by the Animal Care and Use Committee of the National Center for Global Health and Medicine Research Institute and were conducted according to institutional procedures (no. 20050).

Biochemical Analysis. For immunoprecipitation experiments, we used WEHI231 transfectants expressing Myc-tagged mouse SLC15A4 or 293T transfectants transiently overexpressing human or mouse HA-tagged SLC15A4 in combination with Flag-tagged mouse AMPK-α. We collected and lysed the cells 48 h after transfection using digitonin lysis buffer (1% digitonin, 50 mM Tris HCl pH 7.5, 150 mM NaCl, 1 mM $MgCl_2$, 1 mM $CaCl_2$, and 5% glycerol with the 1× Halt Protease Inhibitor Mixture and 1× Halt Phosphatase Inhibitor mixture, both from Thermo Fisher Scientific). The lysates were cleared using a microcentrifuge (13,000 × *g* for 10 min at 4 °C) and incubated with anti-Myc mAb-coupled agarose beads (Fujifilm Wako Chemicals), anti-HA mAb (Fujifilm Wako chemicals), or anti-Flag mAb (M2, Sigma-Aldrich) for 2 h with rotation at 4 °C. The beads were recovered and washed three times with lysis buffer and analyzed by sodium dodecyl sulfate–polyacrylamide gel electrophoresis (SDS-PAGE) and Western blotting.

BioID Analysis. We constructed the BioID.cMyc-BirA-SLC15A4 vector (BioID-SLC15A4) by PCR cloning full-length human SLC15A4 into the pCDNA3.1-cMyc-BirA vector (12) and transfected the vectors into 293T cells using Lipofectamine 3000 Transfection Reagent (Thermo Fisher Scientific) to create a stable inducible cell line; stable cells were selected in 10 μg/mL blastidin. We created a control cell line by transfecting 293T cells with a pCAGGS-Met-Gly-Cys-cMyc-BirA vector (BioID-Control). The MGC motif helps to anchor cMyc-BirA to the cell membrane.

We identified candidate proteins by BioID pull-down as previously described (12). Briefly, we grew BioID-SLC15A4 and BioID-Control 293T cells in 100-mm dishes to ~80% confluency; 24 h before harvesting the cells, the medium was replaced with fresh medium containing 50 μM biotin (Wako Pure Chemical Corporation). The cells were scraped into cold PBS and washed twice with PBS at 4 °C. The cell pellets were resuspended in 2.4 mL lysis buffer consisting of 50 mM Tris Cl pH 7.5, 0.5 M NaCl, 0.4% SDS (weight/volume), 5 mM ethylenediaminetetraacetic acid (EDTA), and 1× Halt Protease Inhibitor mixture (Thermo Fisher Scientific) and then sonicated. Triton X-100 was added to a 2% final concentration. After further sonication, an equal volume of 50 mM Tris pH 7.5 at 4 °C was added before additional sonication and centrifugation (16,000 × *g* for 10 min at 4 °C). The supernatants were incubated with 600 μL Dynabeads (MyOne Streptavidin C1, Thermo Fisher Scientific) overnight at 4 °C. The beads were collected and washed twice with 1 mL wash buffer 1 (2% SDS in dH_2O) followed by washing with wash buffer 2 (0.1% deoxycholate, 1% Triton X-100, 0.5 M NaCl, 1 mM EDTA, and 50 mM Hepes, pH 7.0) and with wash buffer 3 (250 mM LiCl, 0.5% Nonidet P-40, 0.5% deoxycholate, 1 mM EDTA, and 10 mM Tris pH 7.5). The beads were further washed with wash buffer 4 twice (50 mM Tris pH 7.5 with 50 mM NaCl). Finally, the bound proteins were eluted with 100 μL Laemmli SDS sample buffer containing 2 mM biotin at 98 °C.

Mass Spectrometry Analysis. Samples were eluted from streptavidin beads with 100 μL sample buffer for 5 min at 98 °C and were subjected to SDS-PAGE. Electrophoresis was stopped when the protein migrated from the stacking gel to the separation gel, and the gel was stained with Coomassie blue. The protein bands on the top of the separation gel were excised and destained. Protein was digested in a gel containing trypsin (N-Tosyl-L-phenylalanyl chloromethyl ketone treated, Worthington Biochemical Corporation). The digestion mixtures were separated with a nanospray column (NTCC-360/75–3-105, Nikkyo Technos, Co., Ltd.) using EASY-nLC 1200 (Thermo Fisher Scientific) in a gradient of 0 to 64% B buffer per 50 min (0.1% formic acid/80% AcCN) at a flow rate of 300 nl/min. Online mass spectrometry (MS) was conducted with a Q Exactive HFX mass spectrometer (Thermo Fisher Scientific) equipped with a nanospray ion source. The MS and tandem MS (MS/MS) spectra were acquired with the data-dependent TOP10 method, and the obtained data were further analyzed with Proteome Discoverer 2.2 (Thermo Fisher Scientific) using MASCOT version 2.6 (Matrix Science).

Glucose Uptake Assay. Glucose uptake was measured using a Glucose Uptake Cell-Based Assay Kit (Cayman Chemical) according to the manufacturer's instructions. Briefly, CAL-1 cells (2×10^4 cells) were seeded in a 96-well plate with 100 μl complete RPMI medium 1640 and stimulated with 2 μg/mL CpG-B (ODN2006, InvivoGen) at 37 °C for the indicated periods. After stimulation, cells were equilibrated in glucose-free medium for 2 h prior to treatment with 2-NBDG at 100 μg/mL for 10 mins at 37 °C. Cells were washed with cell-based assay buffer, and fluorescence intensity was analyzed on a BD FACSVerse flow cytometer.

Flow Cytometry. Cultured cells or single-cell suspensions prepared from BM were stained with the indicated mAbs in each figure and analyzed by flow cytometry. For intracellular staining, cells were fixed by 4% paraformaldehyde in PBS and permeabilized by 1× BD Perm/Wash (BD Biosciences) prior to staining with the indicated mAbs and with fluorochrome-conjugated secondary antibodies. Fluorescence intensity was analyzed on a BD Biosciences FACSVerse or FACSAria II flow cytometer. For intracellular cytokine staining, BM macrophages were stimulated with CpG for the indicated periods. Monensin (BD Biosciences) was added 3 h prior to harvesting of the cells. Collected macrophages were fixed and permeabilized followed by staining with antibody against Ebi3. Fluorescence intensity was analyzed on a FACSVerse flow cytometer.

Immunoblot Analysis. Whole-cell lysates or immunoprecipitates were subjected to SDS-PAGE electrophoresis and transferred to polyvinylidene difluoride membranes. The membranes were blocked with blocking reagents to prevent non-specific antibody absorption. Immunoblotting was performed using primary antibodies as indicated in each figure followed by horseradish peroxidase–conjugated secondary antibodies. The signal was detected with Supersignal West Femto or Supersignal West Pico chemiluminescent substrates on the LAS-3000 detection system (Fuji Photo Film). Band intensity was quantified with Image Gauge (Fuji Photo Film) or ImageJ (NIH). All antibodies used in this study are listed in *SI Appendix*, Table S1.

Immunohistochemistry. Cells were fixed and permeabilized with the Fixation/Permeabilization Solution Kit (BD Biosciences) for 20 min at 4 °C and then stained with the indicated primary antibodies followed by staining with the following fluorochrome-conjugated secondary antibodies: Alexa Fluor 568 anti-rabbit Ig (H+L), Alexa Fluor 488 anti-chicken IgY, or Alexa Fluor 647 anti-rat Ig (H+L). Subcellular distribution was visualized using a Zeiss

AiryScan confocal microscope (Carl Zeiss AG) and analyzed using the ZEN 2.3 (blue edition) Service Pack 1.

Gene Expression Assays. RNA from cells was purified with the RNeasy Mini Kit (Qiagen) or ISOGEN (Nippon Gene) and reverse transcribed using the LunaScript RT SuperMix Kit (New England Biolabs, Inc.). SYBR-based qPCR was conducted with a StepOne Plus Real-Time PCR System (Thermo Fisher Scientific) with specific primers for human *SLC15A4*, *IFNB*, *IL1B*, or *HPRT*. Gene expression was normalized to *HPRT*. Gene expression analysis for mouse genes was performed with TaqMan probes (Thermo Fisher Scientific) or THUNDERBIRD SYBR green qPCR system (TOYOBO) with the specific primers. The primers used in this study are listed in *SI Appendix*, Table S2.

Cytokine Quantification. We quantified protein concentrations of the cytokines using the following enzyme-linked immunosorbent assay (ELISA) kits: mouse TNF-α with TNF alpha Mouse ELISA Kit (Thermo Fisher Scientific) and mouse IL-12/IL-23 p40 with ELISA MAX Standard Set Mouse IL-12/IL-23 p40 (BioLegend). ELISA was performed according to the manufacturers' protocols.

XF Flux Analysis. CAL-1 cells were seeded in CellTAK-coated XF-96 cell-culture plates (Seahorse Bioscience) at a density of 6×10^4 cells/well on the day of the experiment. BMMɸ were seeded in XF-96 cell-culture plates at a density of 3×10^4 cells/well, incubated overnight, and treated as specified in figure legends. OCR and ECAR were assessed using the XF-96 Flux Analyzer (Seahorse Bioscience) according to the manufacturer's instructions. For Mito Stress Tests, we measured OCR changes in response to oligomycin (1 μM), FCCP (1.5 μM), antimycin A (1 μM) plus rotenone (1 μM), and 2DG (50 mM). In Glyco Stress Tests, we measured changes in ECAR in response to glucose (10 mM), oligomycin (1 μM), and 2DG (50 mM) injection. The fetal calf serum used was dialyzed four times against a 100-fold excess PBS at 4 °C with stirring for at least 2 h per exchange. The data were analyzed using Wave 2.4.0 (Agilent Technology). Values are shown as mean ± SE.

Metabolic Flow Analyses by Liquid Chromatography and MS. Wild-type or *Slc15a4*$^{-/-}$ BMMɸ were seeded at a density of 1.6×10^6 cells in 6-well plates and incubated for the indicated periods with or without CpG1668. In some

experiments, BMMɸ were stimulated in RPMI 1640 Complete Medium containing 1% FBS. After CpG stimulation, culture supernatants were removed, and the cells were further incubated in the presence of $^{13}C_6$-glucose (10 mM) or $^{13}C_5$-glutamine (2 mM) for 1 h. Metabolites were extracted from cultured cells for metabolome analyses as described previously (40, 41). Briefly, the cells were scraped with methanol (500 μL) containing an internal standard, followed by the addition of an equal volume of chloroform and 0.4 volume of ultrapure water (liquid chromatography [LC]/MS grade, Wako) to the aqueous phase to obtain the extracted hydrophilic metabolites. The aqueous phase was ultrafiltered using an ultrafiltration tube (Ultrafree MC-PLHCC; Human Metabolome Technologies), concentrated in a vacuum concentrator, and then dissolved in 50 μL ultrapure water for LC-MS/MS and ion chromatography (IC)-MS analysis. For metabolome analysis, metabolites were measured using an orbitrap-type MS (Q Exactive Focus; Thermo Fisher Scientific) connected to a high-performance IC system (ICS-5000+, Thermo Fisher Scientific) as previously described (40). Values are shown as mean ± SD.

Statistics. We analyzed the significance of differences in the mean ± SD or in the mean ± SE of various groups using Student's two-tailed *t* test unless otherwise noted. $P < 0.05$ was considered statistically significant.

1. R. Stienstra, R. T. Netea-Maier, N. P. Riksen, L. A. B. Joosten, M. G. Netea, Specific and complex reprogramming of cellular metabolism in myeloid cells during innate immune responses. *Cell Metab.* **26**, 142–156 (2017).
2. B. Kelly, L. A. O'Neill, Metabolic reprogramming in macrophages and dendritic cells in innate immunity. *Cell Res.* **25**, 771–784 (2015).
3. T. Kobayashi *et al.*, The histidine transporter SLC15A4 coordinates mTOR-dependent inflammatory responses and pathogenic antibody production. *Immunity* **41**, 375–388 (2014).
4. A. L. Blasius *et al.*, Slc15a4, AP-3, and Hermansky-Pudlak syndrome proteins are required for Toll-like receptor signaling in plasmacytoid dendritic cells. *Proc. Natl. Acad. Sci. U.S.A.* **107**, 19973–19978 (2010).
5. H. Daniel, G. Kottra, The proton oligopeptide cotransporter family SLC15 in physiology and pharmacology. *Pflugers Arch.* **447**, 610–618 (2004).
6. S. Sasawatari *et al.*, The solute carrier family 15A4 regulates TLR9 and NOD1 functions in the innate immune system and promotes colitis in mice. *Gastroenterology* **140**, 1513–1525 (2011).
7. A. L. Blasius, P. Krebs, B. M. Sullivan, M. B. Oldstone, D. L. Popkin, Slc15a4, a gene required for pDC sensing of TLR ligands, is required to control persistent viral infection. *PLoS Pathog.* **8**, e1002915 (2012).
8. L. X. Heinz *et al.*, TASL is the SLC15A4-associated adaptor for IRF5 activation by TLR7-9. *Nature* **581**, 316–322 (2020).
9. R. Baccala *et al.*, Essential requirement for IRF8 and SLC15A4 implicates plasmacytoid dendritic cells in the pathogenesis of lupus. *Proc. Natl. Acad. Sci. U.S.A.* **110**, 2940–2945 (2013).
10. T. Kobayashi *et al.*, Lysosome biogenesis regulated by the amino-acid transporter SLC15A4 is critical for functional integrity of mast cells. *Int. Immunol.* **29**, 551–566 (2017).
11. K. J. Roux, D. I. Kim, M. Raida, B. Burke, A promiscuous biotin ligase fusion protein identifies proximal and interacting proteins in mammalian cells. *J. Cell Biol.* **196**, 801–810 (2012).
12. S. Lahaie *et al.*, The endosomal sorting adaptor HD-PTP is required for ephrin-B:EphB signalling in cellular collapse and spinal motor axon guidance. *Sci. Rep.* **9**, 11945 (2019).
13. M. Cebula, N. Moolla, A. Capovilla, E. S. J. Arnér, The rare TXNRD1_v3 ("v3") splice variant of human thioredoxin reductase 1 protein is targeted to membrane rafts by N-acylation and induces filopodia independently of its redox active site integrity. *J. Biol. Chem.* **288**, 10002–10011 (2013).

14. T. Suzuki, N. Dohmae, SLC15A4 functions as a metabolic guardian of immune cells by controlling mTORC1 and AMPK. ProteomeXchange Consortium. https://www.ebi.ac.uk/pride/archive/projects/PXD020370. Deposited 15 July 2020.
15. T. Maeda *et al.*, A novel plasmacytoid dendritic cell line, CAL-1, established from a patient with blastic natural killer cell lymphoma. *Int. J. Hematol.* **81**, 148–154 (2005).
16. T. Kobayashi *et al.*, Human SLC15A4 is crucial for TLR-mediated type I interferon production and mitochondrial integrity. *Int. Immunol.* **33**, 399–406 (2021).
17. A. S. Divakaruni, A. Paradyse, D. A. Ferrick, A. N. Murphy, M. Jastroch, Analysis and interpretation of microplate-based oxygen consumption and pH data. *Methods Enzymol.* **547**, 309–354 (2014).
18. L. A. O'Neill, R. J. Kishton, J. Rathmell, A guide to immunometabolism for immunologists. *Nat. Rev. Immunol.* **16**, 553–565 (2016).
19. V. Lampropoulou *et al.*, Itaconate links inhibition of succinate dehydrogenase with macrophage metabolic remodeling and regulation of inflammation. *Cell Metab.* **24**, 158–166 (2016).
20. D. G. Ryan, L. A. J. O'Neill, Krebs cycle reborn in macrophage immunometabolism. *Annu. Rev. Immunol.* **38**, 289–313 (2020).
21. Z. Zasłona, L. A. J. O'Neill, Cytokine-like roles for metabolites in immunity. *Mol. Cell* **78**, 814–823 (2020).
22. D. Bastian, Y. Wu, B. C. Betts, X. Z. Yu, The IL-12 cytokine and receptor family in graft-vs.-host disease. *Front. Immunol.* **10**, 988 (2019).
23. J. Blagih *et al.*, The energy sensor AMPK regulates T cell metabolic adaptation and effector responses in vivo. *Immunity* **42**, 41–54 (2015).
24. D. G. Hardie, F. A. Ross, S. A. Hawley, AMPK: A nutrient and energy sensor that maintains energy homeostasis. *Nat. Rev. Mol. Cell Biol.* **13**, 251–262 (2012).
25. G. R. Steinberg, D. Carling, AMP-activated protein kinase: The current landscape for drug development. *Nat. Rev. Drug Discov.* **18**, 527–551 (2019).
26. M. Savini, Q. Zhao, M. C. Wang, Lysosomes: Signaling hubs for metabolic sensing and longevity. *Trends Cell Biol.* **29**, 876–887 (2019).
27. A. S. Chauhan, L. Zhuang, B. Gan, Spatial control of AMPK signaling at subcellular compartments. *Crit. Rev. Biochem. Mol. Biol.* **55**, 17–32 (2020).
28. C. G. McCarthy, C. F. Wenceslau, S. Ogbi, T. Szasz, R. C. Webb, Toll-like receptor 9-dependent AMPKα activation occurs via TAK1 and contributes to RhoA/ROCK signaling and actin polymerization in vascular smooth muscle cells. *J. Pharmacol. Exp. Ther.* **365**, 60–71 (2018).
29. Y. Shintani *et al.*, TLR9 mediates cellular protection by modulating energy metabolism in cardiomyocytes and neurons. *Proc. Natl. Acad. Sci. U.S.A.* **110**, 5109–5114 (2013).

Kobayashi et al.
SLC15A4 mediates M1-prone metabolic shifts in macrophages and guards immune cells from metabolic stress

PNAS | 9 of 10
https://doi.org/10.1073/pnas.2100295118
www.manaraa.com

30. C. S. Zhang *et al.*, The lysosomal v-ATPase-Ragulator complex is a common activator for AMPK and mTORC1, acting as a switch between catabolism and anabolism. *Cell Metab.* **20**, 526–540 (2014).

31. M. Xie *et al.*, A pivotal role for endogenous TGF-beta-activated kinase-1 in the LKB1/AMP-activated protein kinase energy-sensor pathway. *Proc. Natl. Acad. Sci. U.S.A.* **103**, 17378–17383 (2006).

32. M. Miyajima, Amino acids: Key sources for immunometabolites and immuno-transmitters. *Int. Immunol.* **32**, 435–446 (2020).

33. N. J. MacIver, R. D. Michalek, J. C. Rathmell, Metabolic regulation of T lymphocytes. *Annu. Rev. Immunol.* **31**, 259–283 (2013).

34. L. Yang, S. Venneti, D. Nagrath, Glutaminolysis: A hallmark of cancer metabolism. *Annu. Rev. Biomed. Eng.* **19**, 163–194 (2017).

35. A. Viola, F. Munari, R. Sánchez-Rodríguez, T. Scolaro, A. Castegna, The metabolic signature of macrophage responses. *Front. Immunol.* **10**, 1462 (2019).

36. W. Ren *et al.*, Glutamine metabolism in macrophages: A novel target for obesity/type 2 diabetes. *Adv. Nutr.* **10**, 321–330 (2019).

37. R. J. Arts *et al.*, Glutaminolysis and fumarate accumulation integrate im-munometabolic and epigenetic programs in trained immunity. *Cell Metab.* **24**, 807–819 (2016).

38. J. H. Pope, M. K. Horne, E. J. Wetters, Significance of a complement-fixing antigen associated with herpes-like virus and detected in the Raji cell line. *Nature* **222**, 186–187 (1969).

39. M. Yoshizaki *et al.*, Spatiotemporal regulation of intracellular trafficking of Toll-like receptor 9 by an inhibitory receptor, Ly49Q. *Blood* **114**, 1518–1527 (2009).

40. H. Semba *et al.*, HIF-1α-PDK1 axis-induced active glycolysis plays an essential role in macrophage migratory capacity. *Nat. Commun.* **7**, 11635, 10.1038/ncomms11635 (2016).

41. T. Yamamoto *et al.*, Reduced methylation of PFKFB3 in cancer cells shunts glucose towards the pentose phosphate pathway. *Nat. Commun.* **5**, 3480, 10.1038/ncomms4480 (2014).

Kobayashi et al.
SLC15A4 mediates M1-prone metabolic shifts in macrophages and guards immune cells